Characterizing Nonlinear Rate-dependent Behaviors of Graphite/Epoxy Composites using a Micromechanical Approach

Jia-Lin Tsai and Kuei-Han Chen

Journal of Composite Materials 2007 41: 1253
DOI: 10.1177/0021998306067307

Characterizing Nonlinear Rate-dependent Behaviors of Graphite/Epoxy Composites using a Micromechanical Approach

JIA-LIN TSAI* AND KUEI-HAN CHEN
Department of Mechanical Engineering, National Chiao Tung University
Hsinchu, Taiwan, 300

ABSTRACT: This research aims to characterize the nonlinear rate-dependent behaviors of graphite/epoxy composites using micromechanical analysis. In this analysis, graphite fibers are considered as elastic solids, while the surrounding epoxy matrix exhibiting rate sensitivities are described using the three-parameter viscoplasticity model. By using Aboudi's generalized method of cells (GMC), the incremental form of the constitutive relations of the composites are expressed in terms of the constituent properties as well as the geometry parameters of the representative volume element. After a numerical iteration, the corresponding stress and strain relations of composites at different strain rates are generated. In order to verify the model predictions, off-axis graphite/epoxy composite specimens are tested at strain rates from 10^{-4} to 550/s. For strain rates less than 1/s, the experiments are conducted using a hydraulic MTS machine, while high-strain-rate tests were carried out using a split Hopkinson pressure bar. Experimental results indicate that the stress and strain curves are quite sensitive to the strain rate; moreover, when the strain rates increase, the material stiffens. A comparison of model predictions with experimental results indicates that the rate-dependent behaviors of composites can be characterized effectively with the GMC model in conjunction with the viscoplastic properties of epoxy.

KEY WORDS: strain rate, graphite/epoxy composites, viscoplasticity, micromechanical analysis, generalized method of cell (GMC).

INTRODUCTION

COMPOSITE MATERIALS, BECAUSE of their high strength-to-weight ratio, have been extensively used not only in aerospace industries but also in marine and automotive industries. In some applications, such as blast-loading of a submarine hull and bird strike of aircraft structures, high-strain-rate loading may be produced, and it is necessary to

*Author to whom correspondence should be addressed. E-mail: jialin@mail.nctu.edu.tw
Figures 1, 7, 9, 10 and 14 appear in color online: http://jcm.sagepub.com

0021-9983/07/10 1253–21 $10.00/0 DOI: 10.1177/0021998306067307

realize the high-strain-rate responses of composite materials. It is well known that polymer materials generally demonstrate strain rate sensitivity. For polymeric composites, the associated deformations dominated by the polymer matrix may also be affected by strain rates. In past decades, the nonlinear rate-dependent behaviors of composites have been studied by many researchers who treated the unidirectional composites as orthotropic homogeneous solids [1–5]. However, such a macromechanical approach cannot yield a specific characterization of the effects of constituent properties on the mechanical behaviors of composites. In order to investigate the influences of ingredients on the mechanical properties of composites, we applied a micromechanical approach in which the composite was treated as a non-homogeneous solid consisting of fiber and matrix phases. Based on the assumption of repeating characteristics of the microstructures, the whole fiber composites could be approximated by a representative volume element (RVE). From the micromechanical analysis of RVE, the overall composite properties were determined. There are several micromechanical models available for describing the mechanical behaviors of composites, i.e., Eshelby's model [6], Mori–Tanaka's model [7,8], the square-fiber model [9], and the generalized method of cells (GMC) [10–12].

Eshelby [6] introduced Eshelby's tensor together with the equivalent principle concept to model a homogeneous inclusion embedded in an infinite matrix. Basically, Eshelby's model is a dilute model with only one inclusion considered. Mori and Tanaka [7] extended Eshelby's approach to establish a nondilute model in which the stress and strain states of the inclusion as well as the matrix are considered in an average sense. Afterward, Benveniste [8] provided alternative explanations of Eshelby's model and the Mori–Tanaka model by introducing the strain concentration concept, and obtained a succinct formulation for these two models. Sun and Chen [9] proposed a two-dimensional (2-D) square-fiber model with three sub-regions under plane stress conditions to model nonlinear behaviors of unidirectional fiber composites. In their model, the fiber is considered to be linear elastic, and the matrix is assumed to follow the nonlinearity of von Mises J_2 materials. Aboudi [10,11] derived a four subcell micromechanical model, method of cells, which is very efficient in modeling the elastic and inelastic behavior of fiber-reinforced composites. Based on the displacement and traction continuity at the interfaces of all subcells as well as the periodicity conditions of RVE, a constitutive relation for the composite materials was derived. By extending the method of cells, Paley and Aboudi [12] proposed a scheme called the generalized method of cells (GMC) to deal with the RVE with complex microstructures. However, because a large number of subcells were generated in the RVE, a great deal of computation is required to implement the GMC model. To enhance the computational efficiency of GMC, Pindera and Bednarcyk [13] proposed a modified formulation of GMC such that the efficiency in the computation of GMC is enhanced substantially. Ogihara et al. [14] employed the GMC model to characterize the nonlinear behavior of unidirectional carbon–epoxy laminates subjected to off-axis loading. For the angle-ply laminates, the behaviors were predicted using the one-parameter plasticity model. In view of the above, most micromechanical analyses mainly focus on the quasi-static behaviors of fiber composites.

On the other hand, very little research has been reported regarding the strain rate effect. Goldberg and Stouffer [15] adopted a four-region micromechanical model to generate the constitutive relations of the composites at different strain rates. In their analysis, the matrix properties are modeled by using a modification of Bodner and Partom's model originally developed by Stouffer and Dame [16], and the stress and strain curves of composites are then obtained by solving systems of differential equations.

Robertson and Mall [17,18] proposed a 3-D micromechanical formulation for fiber composites with plastic–viscoplastic matrix properties. The nonlinear responses of composites under various cyclic loading conditions were predicted accurately by their analysis. Kawai et al. [19] investigated the AS4/PEEK composites with loading and unloading conditions at a strain rate up to 0.01/min. The PEEK matrix is described by the Chaboche model, and the composite behaviors are predicted using GMC. Nevertheless, the corresponding strain rates in their investigations are not high enough for engineering applications.

The objective of this study is to propose a systematic characterization of the high-strain-rate responses of graphite/epoxy composites using the micromechanical approach in conjunction with the rate-dependent behaviors of the epoxy matrix. The rate sensitivities of the epoxy phase is described by a simple constitutive model proposed based on low-strain-rate tests. In addition, the graphite fiber is assumed to be a transverse isotropic solid [20]. With the corresponding ingredient properties, the constitutive behaviors of graphite/epoxy composites at various strain rate ranges were generated using the GMC micromechanical model. In order to verify the model predictions, off-axis graphite/epoxy composites were tested at strain rates that range from 10^{-4} to 550/s. The experimental stress and strain curves were then compared to the predictions obtained from the micromechanical model.

CHARACTERIZING RATE-DEPENDENT BEHAVIORS OF EPOXY

To model the rate-dependent behaviors of fiber composites using micromechanical analysis, the ingredient properties associated with rate sensitivity need to be determined initially. In a graphite/epoxy composite, the graphite fiber in general does not rely on strain rate. In contrast, the epoxy matrix is quite sensitive to the strain rate such that rate-dependent behaviors need to be introduced in the constitutive relation. In an effort to achieve the purpose, epoxy samples were tested in compression under three different strain rates, the results of which formed the basis for the development of a simple elastic–viscoplastic constitutive model of epoxy.

Material Preparations and Experimental Procedures

The epoxy resin adopted in the experiment is the same as the matrix material employed in the prepreg (PPG) graphite/epoxy composites. Both the epoxy resin and the PPG graphite/epoxy composites were supplied by Ad-group Corp, Taiwan. The epoxy resin was originally in the form of powder and stored at a low temperature. The cylindrical epoxy specimens, 10 mm in length and 12 mm in diameter, were prepared by pouring the epoxy powder into a customized Teflon mold, followed by a recommended curing process in a vacuum oven. To achieve consistent material properties, the curing process used for the fabrication of PPG graphite/epoxy composites was employed in the preparation of the epoxy specimens. After curing, the cylindrical samples were lapped on a lapping machine with 15 μm abrasive slurry to yield smooth and flat loading surfaces.

Compression tests were performed on cylindrical specimens using a hydraulic MTS machine. A self-adjusting device as shown in Figure 1 was used to eliminate potential bending and also to ensure the specimen stays in full contact with the loading fixture. During the tests, the contact interfaces between the specimens and the loading fixture were

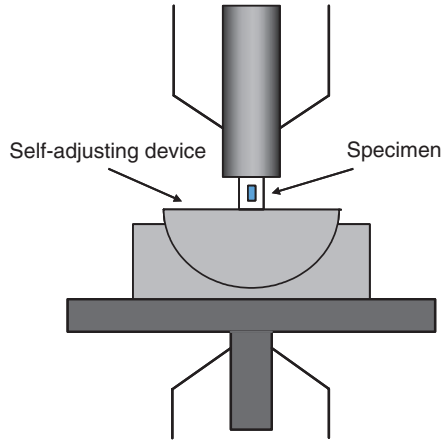

Figure 1. *Schematic of the compression test.*

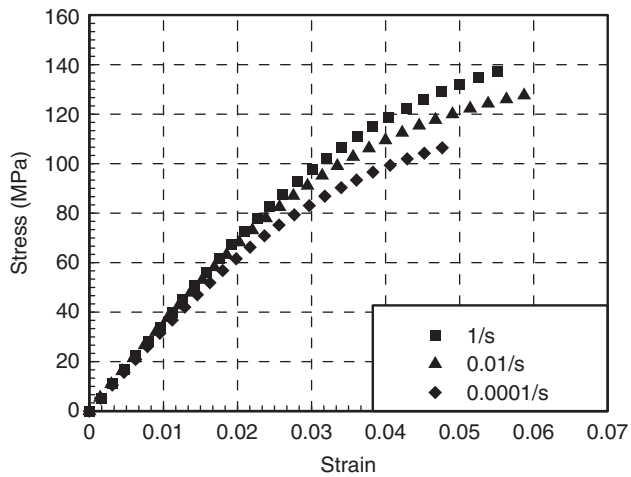

Figure 2. *Stress and strain curves for epoxy specimens at three different strain rates.*

lubricated to reduce friction. The experiments were conducted under the stroke-control mode at three different nominal strain rates, 10^{-4}, 10^{-2}, and 1/s. The nominal strain rate is the stroke rate of the loading frame divided by the original specimen length. It is noted that the corresponding true strain rates were measured using strain gages directly mounted back-to-back on the specimens. Results indicate that the true strain is quite different from the nominal strain; thus, the true strain rate is also different from the nominal strain rate. The discrepancy could be attributed to the self-adjusting device implemented in the compression tests. In the present study, the strain histories measured directly from the strain gages were adopted to generate the stress and strain curves of the epoxy.

Figure 2 shows the measured stress–strain curves for the epoxy specimens at three different nominal strain rates. It was revealed that the elastic modulus of the material is not affected appreciably by strain rate, but the nonlinear deformation is quite sensitive

to strain rate. Thus, an elastic–viscoplastic constitutive model is required to characterize such rate-dependent behaviors, and a plastic function is desired to describe plastic behavior. It is noted that, in material characterization, nonlinear deformation is assumed to be a plastic deformation; thus, the associated behavior could be described using the plasticity theory although the unloading process has not been performed in the compression experiments. Moreover, the unloading process is nonlinear, which is not accounted for in the constitutive model.

Viscoplasticity Model

To model the nonlinear deformation, the epoxy material was assumed to follow the nonlinearity of von Mises J_2 material, and through the flow rule, the plastic strain rate was expressed as

$$\dot{\varepsilon}_{ij}^{p} = \dot{\lambda}\frac{\partial J_2}{\partial \sigma_{ij}} \tag{1}$$

where

$$J_2 = \frac{1}{6}\left[(\sigma_{11}-\sigma_{22})^2+(\sigma_{22}-\sigma_{33})^2+(\sigma_{33}-\sigma_{11})^2\right]+\sigma_{12}^2+\sigma_{23}^2+\sigma_{13}^2 \tag{2}$$

and $\dot{\lambda}$ is a proportionality factor.

By defining an effective stress $\bar{\sigma}$ as

$$\bar{\sigma} = \sqrt{3J_2} \tag{3}$$

through the equivalence of plastic work, i.e.,

$$\dot{W}^{p} = \sigma_{ij}\dot{\varepsilon}_{ij}^{p} = \bar{\sigma}\overline{\dot{\varepsilon}^{p}} = 2J_2\dot{\lambda} \tag{4}$$

the effective plastic strain rate $\overline{\dot{\varepsilon}^{p}}$ was given explicitly as

$$\overline{\dot{\varepsilon}^{p}} = \frac{2}{3}\left\{\frac{1}{2}\left[\left(\dot{\varepsilon}_{11}^{p}-\dot{\varepsilon}_{22}^{p}\right)^2+\left(\dot{\varepsilon}_{22}^{p}-\dot{\varepsilon}_{33}^{p}\right)^2+\left(\dot{\varepsilon}_{33}^{p}-\dot{\varepsilon}_{11}^{p}\right)^2\right]+\frac{3}{4}\left(\dot{\gamma}_{12}^{p2}+\dot{\gamma}_{23}^{p2}+\dot{\gamma}_{13}^{p2}\right)\right\}^{1/2} \tag{5}$$

and the proportionality factor $\dot{\lambda}$ in Equation (1) was derived as

$$\dot{\lambda} = \frac{3}{2}\frac{\overline{\dot{\varepsilon}^{p}}}{\bar{\sigma}} = \frac{3}{2}\frac{\dot{\bar{\sigma}}}{H_p\bar{\sigma}} \tag{6}$$

where H_p

$$H_p = \frac{\dot{\bar{\sigma}}}{\overline{\dot{\varepsilon}^{p}}} \tag{7}$$

is the rate-dependent plastic modulus.

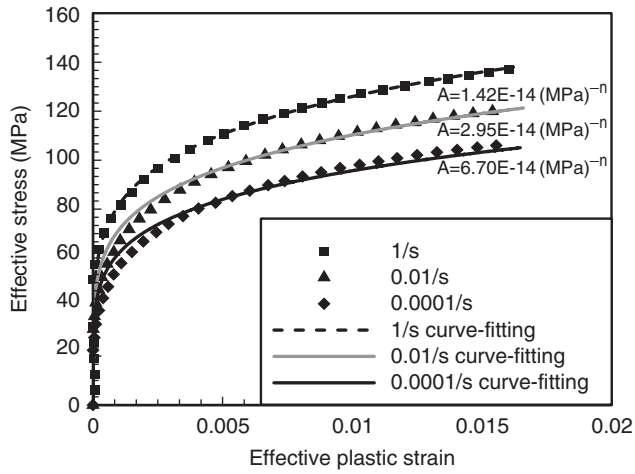

Figure 3. *Effective stress–effective plastic strain curves for epoxy at three different strain rates.*

It is noted that, for the J_2 material subjected to uniaxial loading, the effective stress is equal to the axial stress and the corresponding effective plastic strain is equal to the axial plastic strain ε_x^p obtained by subtracting the elastic part from the total measured strain ε_x. As a result, the effective stress and effective plastic strain curves of the epoxy can be obtained directly from the axial stress and axial plastic strain curves. Figure 3 shows the effective stress and effective plastic strain curves measured at nominal strain rates of 0.0001, 0.01, and 1/s.

To model the effective stress–effective plastic strain curves, a power law function expressed as

$$\overline{\varepsilon^p} = A(\bar{\sigma})^n \tag{8}$$

was used to curve-fit the experimental data as shown in Figure 3. It was observed that the power n in Equation (8) is constant for all tested strain rates. However, the amplitude A is a function of strain rate. Again, a power law was employed to express the amplitude A in terms of effective plastic strain rate as

$$A = \chi\left(\overline{\dot{\varepsilon}^p}\right)^m. \tag{9}$$

By combining Equations (8) and (9), a viscoplasticity model relating the effective stress and effective plastic strain is written as

$$\bar{\varepsilon}^p = \chi\left(\overline{\dot{\varepsilon}^p}\right)^m(\bar{\sigma})^n. \tag{10}$$

It is noted that the effective stress and effective plastic strain curves plotted in Figure 3 were produced for respective constant nominal strain rates but not for constant effective plastic strain rates as required in the viscoplasticity model. By subtracting the elastic component from the total strain, the plastic strain components and thus the effective plastic strains were deduced. Figure 4 shows the effective plastic strain versus time curves

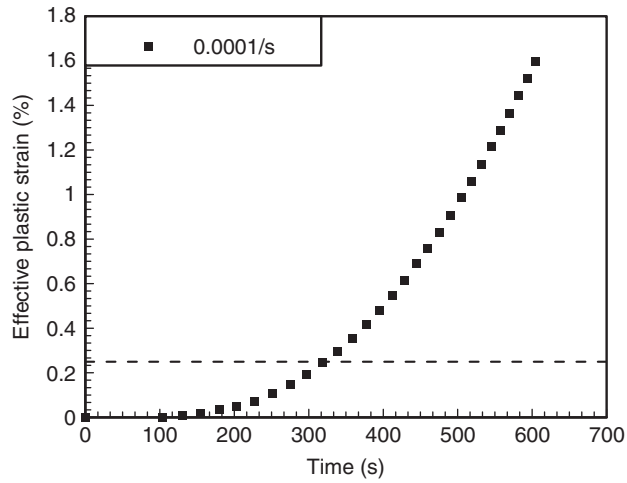

Figure 4. *Effective plastic strain vs time curve for epoxy at a strain rate of 0.0001/s.*

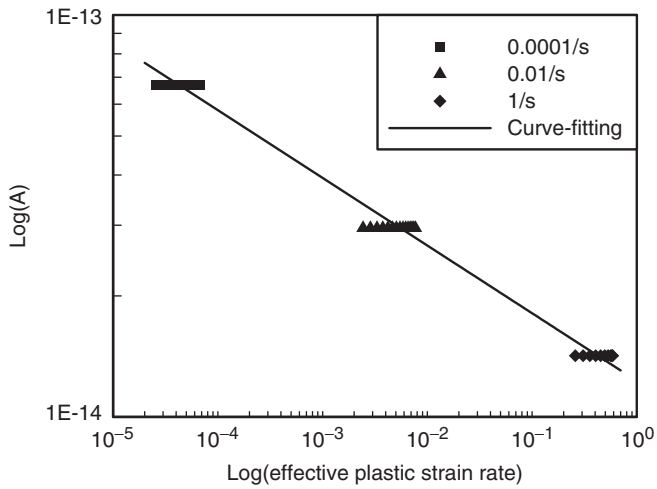

Figure 5. *Log–log plot for determining the parameters in the viscoplasticity model.*

for epoxy specimens associated with a nominal strain rate of 0.0001/s. It is shown that the effective plastic strain rate is not constant over the entire loading range. Nevertheless, it almost reaches a constant value when the effective plastic strain is beyond 0.25%, as indicated by the dash line. Since the initial deformation of the stress–strain curve is mainly dominated by the elastic response, when we determined parameters χ and m in Equation (9) the data in the initial portion where the effective plastic strain is less than 0.25% were truncated. Figure 5 shows amplitude A as a function of effective plastic strain rate on the log–log scale for the epoxy material obtained from the low strain rate compression tests. The parameters χ and m are then determined from these plots as the intercept and the slope, respectively. Once m and χ are determined, this model can be extrapolated to predict the material behavior at various strain rates. The values of the parameters in the viscoplasticity model for epoxy are listed in Table 1.

Table 1. Material properties for the fiber and epoxy used in the micromechanical analysis.

Property (unit)	Fiber	Epoxy
E_1(GPa)	235	3.4
E_2(GPa)	18	
G_{12}(GPa)	35	
G_{23}(GPa)	7.2	
ν_{12}	0.2	0.37
ν_{23}	0.25	
α (1/°C)		5.9×10^{-5}
n		5.62
χ (MPa)$^{-n}$		1.23×10^{-14}
m		−0.168

With Equation (10), the rate-dependent plastic modulus given in Equation (7) is expressed as

$$H_p = \frac{1}{n\chi(\bar{\dot{\varepsilon}}^p)^m(\bar{\sigma})^{n-1}}. \tag{11}$$

Furthermore, from the definition of the effective stress given in Equation (3), $\dot{\bar{\sigma}}$ is derived explicitly as

$$\begin{aligned}\dot{\bar{\sigma}} = \frac{1}{2\bar{\sigma}}\big[&(2\sigma_{11}-\sigma_{22}-\sigma_{33})\dot{\sigma}_{11} + (-\sigma_{11}+2\sigma_{22}-\sigma_{33})\dot{\sigma}_{22} + (-\sigma_{11}-\sigma_{22}+2\sigma_{33})\dot{\sigma}_{33} \\ &+ 6\sigma_{23}\dot{\sigma}_{23} + 6\sigma_{13}\dot{\sigma}_{13} + 6\sigma_{12}\dot{\sigma}_{12}\big].\end{aligned} \tag{12}$$

By substituting Equation (12) together with Equation (6) into Equation (1), the plastic strain rate is written explicitly as

$$\begin{Bmatrix}\dot{\varepsilon}^p_{11}\\ \dot{\varepsilon}^p_{22}\\ \dot{\varepsilon}^p_{33}\\ \dot{\gamma}^p_{23}\\ \dot{\gamma}^p_{13}\\ \dot{\gamma}^p_{12}\end{Bmatrix} = \frac{9}{4}\frac{1}{H_p\bar{\sigma}^2}\begin{bmatrix} S_1^2 & S_1S_2 & S_1S_3 & S_1S_4 & S_1S_5 & S_1S_6 \\ & S_2^2 & S_2S_3 & S_2S_4 & S_2S_5 & S_2S_6 \\ & & S_3^2 & S_3S_4 & S_3S_5 & S_3S_6 \\ & \text{symmetric} & & S_4^2 & S_4S_5 & S_4S_6 \\ & & & & S_5^2 & S_5S_6 \\ & & & & & S_6^2 \end{bmatrix}\begin{Bmatrix}\dot{\sigma}_{11}\\ \dot{\sigma}_{22}\\ \dot{\sigma}_{33}\\ \dot{\sigma}_{23}\\ \dot{\sigma}_{13}\\ \dot{\sigma}_{12}\end{Bmatrix} \tag{13}$$

where

$$\begin{aligned} S_1 &= \frac{1}{3}(2\sigma_{11}-\sigma_{22}-\sigma_{33}) \\ S_2 &= \frac{1}{3}(-\sigma_{11}+2\sigma_{22}-\sigma_{33}) \\ S_3 &= \frac{1}{3}(-\sigma_{11}-\sigma_{22}+2\sigma_{33}) \\ S_4 &= 2\sigma_{23} \\ S_5 &= 2\sigma_{13} \\ S_6 &= 2\sigma_{12}. \end{aligned}$$

It is noted that, in Equation (13), the plastic compliance matrix is dependent on not only the current stress states but also on the strain rate. For a given loading history, a numerical iteration process is usually required to update the compliance matrix. By combining the elastic parts, the incremental form of the constitutive relation of the epoxy material is established as

$$\{\dot{\varepsilon}\} = \left[\mathbf{S}^M\right]\{\dot{\sigma}\} \tag{14}$$

where

$$\left[\mathbf{S}^M\right] = [\mathbf{S}^e] + [\mathbf{S}^p]. \tag{15}$$

In Equation (15), $[\mathbf{S}^e]$ represents the elastic compliance matrix of the epoxy, and $[\mathbf{S}^p]$ denotes the plastic compliance matrix given in Equation (13). By inverting Equation (14), the stress and strain relation expressed in terms of the stiffness matrix is deduced as

$$\{\dot{\sigma}\} = \left[\mathbf{C}^M\right]\{\dot{\varepsilon}\} \tag{16}$$

where

$$\left[\mathbf{C}^M\right] = \left[\mathbf{S}^M\right]^{-1}. \tag{17}$$

Figure 6 demonstrates the model predictions obtained from the viscoplasticity model in comparison with the experimental data. Good agreement in the stress and strain curves was achieved suggesting that the constitutive relations proposed based on viscoplasticity theory are capable of characterizing the rate dependence of the epoxy resin.

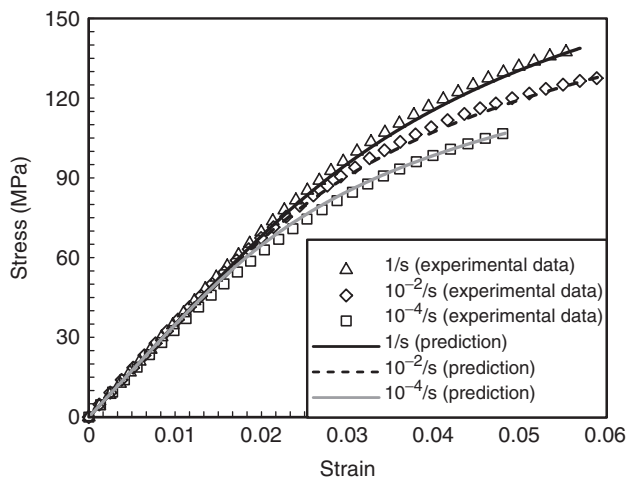

Figure 6. *Verification of the viscoplasticity model for characterizing epoxy at three different strain rates.*

MICROMECHANICAL ANALYSIS

Selection of Representative Volume Element (RVE)

In modeling the mechanical responses of fiber composites using a micromechanical approach, a unit cell needs to be selected properly to represent the microstructures of the materials. In reality, the fibers are displaced randomly within the matrix. However, for the purpose of simplicity, the fibers were assumed to be distributed uniformly and displaced regularly in the form of the square edge array in the matrix such that a unit cell as shown in Figure 7 (enclosed with dash lines) was selected as a RVE for the micromechanical analysis. With the RVE, the GMC proposed by Paley and Aboudi [12] was adopted to characterize the constitutive behaviors of the fiber composites. It is noted that in the GMC analysis, the RVE is divided into numbers of subcells, and the number of the subcells is determined by the fiber geometry. In general, when the round fiber is considered, a significant number of subcells are required in an attempt to precisely simulate the circular geometry of the fiber. Nevertheless, as more subcells are taken into account, more computation time is needed. Figure 8 demonstrates the 20×20 subcells in the RVE, in which the gray ones denote the fibers and the white ones are the surrounding matrix. On the other hand, if the round fiber in the composites can be approximated by a square one with a cross-section equal to that of the circular fiber, the unit cell as shown in Figure 9 (enclosed by the dash line) can be selected as an RVE, and only 2×2 subcells as shown in Figure 10 are adequate for the GMC micromechanical analysis. By this method, the computations necessary can be dramatically reduced. To rationalize this approximation, the stress and strain curves obtained from the unit cells with a square fiber must be verified. The validation can be processed by comparing the results obtained from the RVEs given in Figures 8 and 10.

Figures 11 and 12 demonstrate the stress and strain curves for the 15, 30, 45, and 60° fiber composites obtained from the GMC analysis with the RVE containing the square fiber and the round fiber, respectively, at strain rate of 10^{-4}/s. It was shown that for most fiber orientations, the constitutive curves calculated from both RVEs coincide quite well. The only exception is the 60° specimens, for which a small discrepancy is observed at high strain levels. However, the difference is not critical for engineering

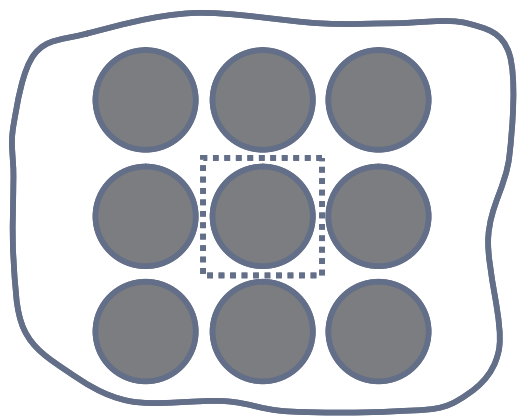

Figure 7. *Square edge array of the round fibers in composites.*

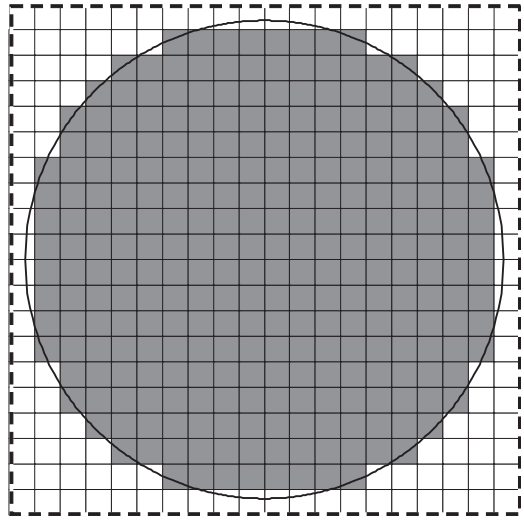

Figure 8. *Selection of RVE with round fibers.*

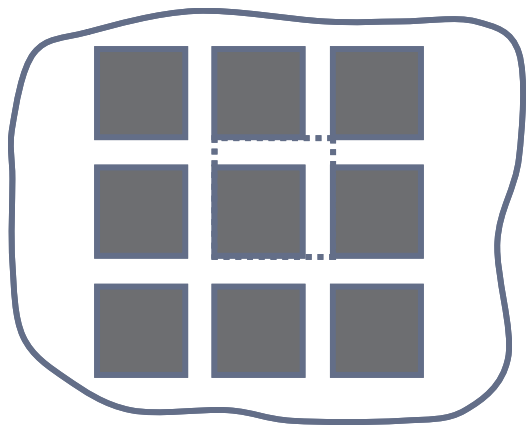

Figure 9. *Square edge array of the square fibers in composites.*

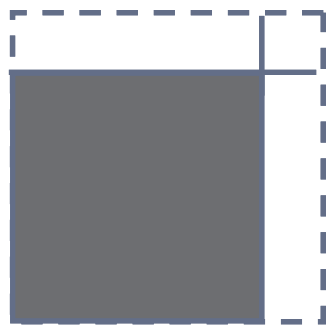

Figure 10. *Selection of RVE with square fibers.*

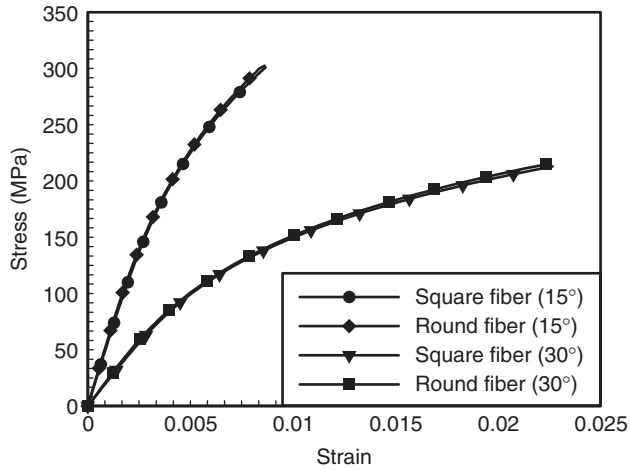

Figure 11. *Fiber-shape effect on the stress and strain curves of 15° and 30° specimens in the GMC analysis.*

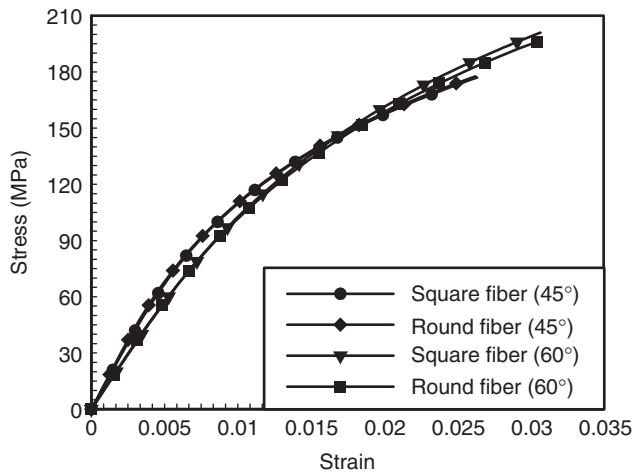

Figure 12. *Fiber-shape effect on the stress and strain curves of 45° and 60° specimens in the GMC analysis.*

applications since the 60° specimens fail before such a high strain level is achieved. The above examinations show that the RVE with square fibers can be employed rather than that with round fibers in the GMC analysis for modeling the mechanical responses of fiber composites.

GMC Micromechanical Model

When a RVE is selected in GMC analysis, it is usually divided into $N_\beta \times N_\gamma$ subcells as shown in Figure 13. Based on the displacement continuity as well as the traction continuity on the interface of the adjacent subcells in conjunction with the periodicity

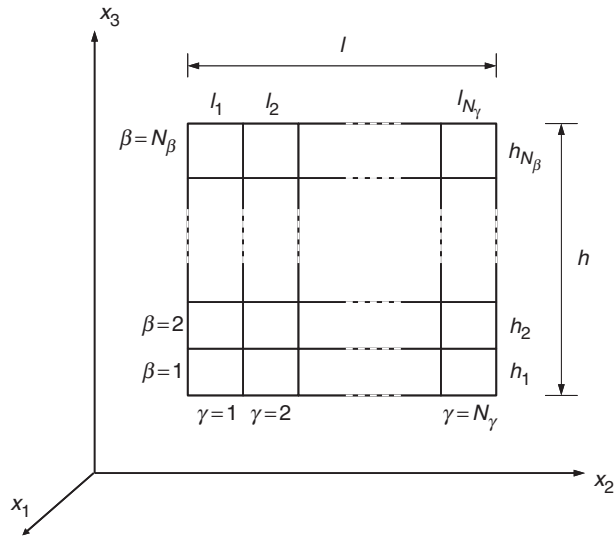

Figure 13. *A typical RVE containing $\mathbf{N}_\beta \times \mathbf{N}_\gamma$ subcells in the GMC analysis [12].*

condition of the RVE, the relation between overall strain rates and subcell strain rates is expressed as [12]

$$\eta_s = \mathbf{A}^{VP}\bar{\eta} \tag{18}$$

where $\eta_s = \{\bar{\eta}^{(11)}, \bar{\eta}^{(12)}, \ldots, \bar{\eta}^{(N_\beta N_\gamma)}\}$ represents the collections of the strain rates for all subcells, and $\bar{\eta} = (\bar{\eta}_{11}, \bar{\eta}_{22}, \bar{\eta}_{33}, 2\bar{\eta}_{23}, 2\bar{\eta}_{13}, 2\bar{\eta}_{12})$ indicates the overall strain rates of the RVE. It is noted that $\mathbf{A}^{VP}$ is a $6\,N_\beta N_\gamma \times 6$ matrix containing the geometry parameters of the RVE and the associated subcells. The $\mathbf{A}^{VP}$ matrix can be partitioned into the $N_\beta N_\gamma$ entries, and each entry represents a 6×6 square matrix as

$$\mathbf{A}^{VP} = \begin{bmatrix} \mathrm{A}^{VP(11)} \\ \mathrm{A}^{VP(12)} \\ \vdots \\ \mathrm{A}^{VP(N_\beta N_\gamma)} \end{bmatrix} \tag{19}$$

Thus, the strain rate components in the subcells can be expressed explicitly in terms of the overall strain rates as

$$\bar{\eta}^{(\beta\gamma)} = \mathbf{A}^{VP(\beta\gamma)}\bar{\eta} \tag{20}$$

where $\beta = 1, \ldots, N_\beta$ and $\gamma = 1, \ldots, N_\gamma$. The constitutive equations of each subcell (β, γ) are written as

$$\bar{\tau}_{ij}^{(\beta\gamma)} = \mathbf{C}_{ijkl}^{VP(\beta\gamma)}\bar{\eta}_{kl}^{(\beta\gamma)} \tag{21}$$

where $\mathbf{C}_{ijkl}^{VP(\beta\gamma)}$ denotes the stiffness matrix of the subcell (β, γ). It is noted that, when the subcells are represented as epoxy material, the stiffness matrix $\mathbf{C}^{VP(\beta\gamma)}$ is the same as that given by Equation (17). When the subcells are denoted as fibers, $\mathbf{C}^{VP(\beta\gamma)}$ represents the elastic stiffness matrix of the fiber. By substituting Equation (20) into the subcell constitutive relation shown in Equation (21), the subcell stress rates are deduced as

$$\bar{\tau}^{(\beta\gamma)} = \mathbf{C}^{VP(\beta\gamma)}\mathbf{A}^{VP(\beta\gamma)}\bar{\eta}. \tag{22}$$

Based on the average sense, the overall stress rate of the RVE is written as

$$\bar{\tau} = \frac{1}{hl}\sum_{\beta=1}^{N_\beta}\sum_{\gamma=1}^{N_\gamma} h_\beta l_\gamma \bar{\tau}^{(\beta\gamma)}. \tag{23}$$

With Equations (22) and (23), the overall stress rate and strain rate relation of the RVE are established as

$$\bar{\tau} = \mathbf{B}^{*VP}\bar{\eta} \tag{24}$$

where

$$\mathbf{B}^{*VP} = \frac{1}{hl}\sum_{\beta=1}^{N_\beta}\sum_{\gamma=1}^{N_\gamma} h_\beta l_\gamma \mathbf{C}^{VP(\beta\gamma)}\mathbf{A}^{VP(\beta\gamma)}. \tag{25}$$

With ingredient properties as well as RVE geometry, Equation (25) can be used to model the responses of fiber composites. All the ingredient properties of the graphite/epoxy composites obtained from low-strain-rate tests are summarized in Table 1. In addition, as a result of fewer computations, only square fibers embedded in the RVE were considered for the analysis; thus, the values of N_β and N_γ in Equation (25) were set to 2 corresponding to the RVE with 2×2 subcells as shown in Figure 10. It is noted that since our rate-dependent constitutive model of the matrix can be simply implemented into the original GMC model, in this study the micromechanical analysis was performed based on the original version of GMC rather than the reformulated one made by Pindera and Bednarcyk [13].

For unidirectional fiber composites, the coefficients of thermal expansion (CTE) of the fiber and the surrounding matrix are quite different. Because of the mismatch of the CTE, thermal residual stresses were produced within the constituents during the curing process, affecting the mechanical behaviors of composites. Thus, the effect of thermal residual stresses needs to be taken into account in the material simulation. By following the experimental procedures proposed in [21], the thermal expansion coefficient α for epoxy resin was measured, and the result is addressed in Table 1. For the graphite fiber, since the CTE is quite small, the value is assumed to be zero in the calculation of the residual stresses. For graphite/epoxy composites, the curing temperature is 150°C, at which point the composites are considered to be stress free. Through thermal-elastic analysis, the thermal residual stresses of the epoxy at room temperature (25°C) were computed and then employed as initial stress variables in the GMC analysis before the mechanical loading was applied.

OFF-AXIS COMPRESSION TESTS

In an effort to verify the model predictions, off-axis block PPG graphite/epoxy composite specimens were tested at various strain rates. For high-strain-rate tests, experiments were conducted using a split Hopkinson pressure bar (SHPB). Alternatively, lower-strain-rate experiments were performed using the hydraulic MTS machine.

Preparation of Graphite/Epoxy Composite Specimens

Off-axis block specimens of $0.6 \times 0.6 \times 1$ cm with fiber orientations of 15, 30, 45, and 60° were cut from a 45-ply unidirectional PPG graphite/epoxy laminate using a diamond wheel. The PPG graphite/epoxy composites consisting of HTA-12K fiber (Toho, Japan) were provided by Ad-group, Taiwan. In order to reduce contact friction between the specimen and the loading frame, the block specimens were lapped on a lapping machine with 14.5 μm abrasive slurry and also lubricated during the tests. In general, the lapping and lubricating process work well for glass–epoxy composites to reduce contact friction. However, for graphite/epoxy composites, because of the stiffer graphite fiber, contact friction is difficult to reduce effectively by the lapping process, resulting in nonhomogeneous deformation during off-axis compression tests. In order to significantly diminish the contact friction, more surface treatments on the loading faces are required for the graphite/epoxy composites. Bing and Sun [22] suggest that in addition to lapping and lubricating, surface-coating with a thin titanium film on graphite/epoxy specimens may be effective in lessening friction. Therefore, all off-axis graphite/epoxy specimens were coated with approximately 1.2 μm titanium film on the loading surfaces using sputtering technology.

Low-strain-rate Tests

Low-strain-rate tests were conducted on the off-axis block specimens using the stroke-control mode on a servo-hydraulic MTS machine (MTS 810 system). Basically, the experimental setup is the same as that used for testing epoxy specimens. Three different nominal strain rates of 10^{-4}, 10^{-2}, and 1/s were implemented for testing the off-axis graphite/epoxy composite specimens. The corresponding true-strain histories were measured by strain gages that were adhered back-to-back to the specimens; concurrently, the applied-load histories were evaluated through load cells mounted onto the loading frame. Stress and strain signals were recorded both by LabView and a personal computer.

High-strain-rate Tests

The high-strain-rate compression tests were performed on the off-axis block specimens using a SHPB, a simple and effective apparatus for dynamic testing. Figure 14 shows the schematic of a conventional SHPB setup made of hardened steel bars 13 mm in diameter. The striker bar was 9.2 cm long, and the incident bar and transmission bar were 92 cm and 58 cm long, respectively. A pair of diametrically opposite gages (gage A) were mounted on

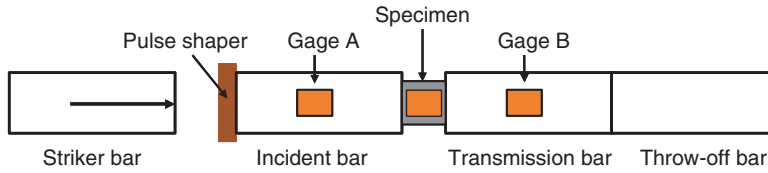

Figure 14. *The SHPB apparatus.*

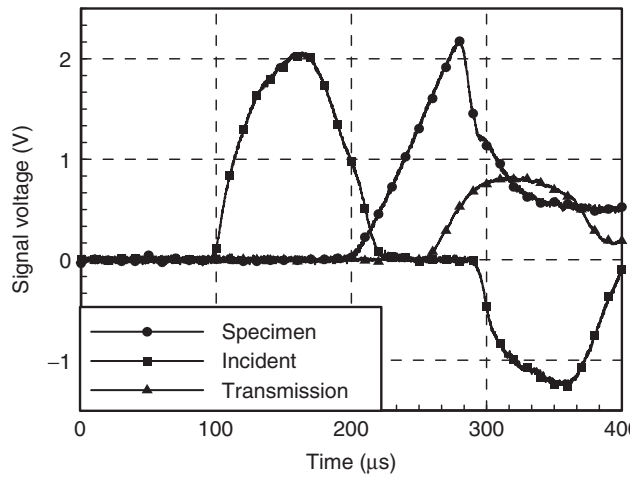

Figure 15. *Strain gage signals recorded in the SHPB test for 30° graphite/epoxy specimens.*

the incident bar to measure both the incident and reflection signals. On the transmission bar, strain gages (gage B) were mounted about 29 cm from the specimen interface to measure the transmitted pulse. The dimensions of the composite specimens for SHPB tests were the same as those used in low-strain-rate tests. The strain-gaged block specimens were sandwiched between the incident bar and the transmission bar, and the strain history of the specimen was obtained directly from the strain gages mounted on the specimen. The strain gages that were adhered to the specimen and bars, respectively, were connected to Wheatstone circuits and then amplified. A pulse shaper was used to produce a gently rising loading pulse that would help in extracting reliable stress–strain curves from SHPB tests [23]. This pulse-shaping technique can be achieved using a piece of soft material inserted between the striker bar and the incident bar. A copper tab 1.7 mm thick was used as the pulse shaper in the present study.

Figure 15 shows the typical strain gage signals measured from the incident and transmission bars and the specimen, respectively, for the 30° graphite/epoxy composites. By using the Hopkinson bar theory [24], the contact force P_1 between the incident bar and the specimen and the contact force P_2 between the specimen and the transmission bar can be extracted from the recorded pulse data. The contact forces P_1 and P_2 for the 30° graphite/epoxy composites are shown in Figure 16. It is noted that P_1 and P_2 almost coincide with each other except that P_1 exhibits greater oscillations than P_2. In view of these oscillation, we took P_2 to calculate the compressive stress in the specimen to generate the dynamic stress–strain curve.

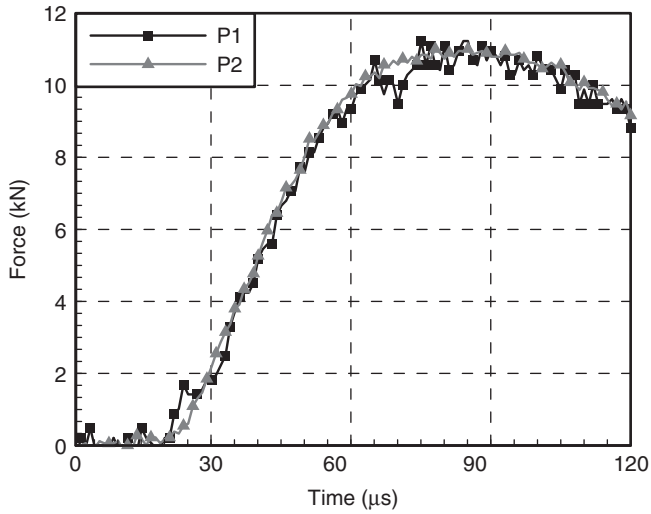

Figure 16. *Time histories of the contact forces for 30° graphite/epoxy specimen during the SHPB tests.*

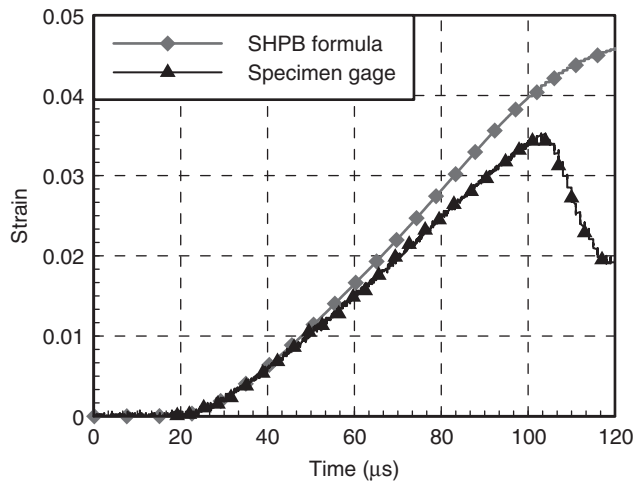

Figure 17. *Strain histories obtained from the Hopkinson bar formula and the specimen gage signal for 30° graphite/epoxy specimen during the SHPB tests.*

Conventionally, the strain history of the specimen during loading can also be calculated using the Hopkinson bar formula with expressions of displacements at the ends of the bars derived from the strain responses recorded at gage A and gage B [24]. In the present study, the strain response of the specimen was also measured using a strain gage directly mounted onto the specimen. Figure 17 shows the comparison of the strain histories for the composite obtained using the Hopkinson bar formula and the strain gage directly mounted onto the specimen, respectively. It is evident that the strain history calculation based on the Hopkinson bar theory deviates from that directly measured on the specimen. In this study, the strain history measured on the specimen was adopted for the generation

of dynamic stress–strain curves. The strain rate ranges measured in the SHPB tests were 225–550/s.

RESULTS AND DISCUSSION

Experimental stress and strain curves of graphite/epoxy composites with fiber orientations of 15, 30, 45, and 60° at various strain rates are shown in Figures 18–21, respectively. Experimental results indicate that the stress and strain curves are quite sensitive to strain rates; moreover, as the strain rate increases, the materials stiffen.

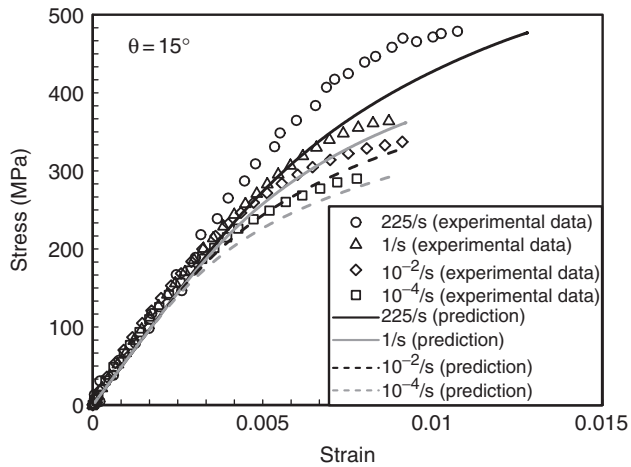

Figure 18. *Comparison of the experimental data with the model predictions for 15° graphite/epoxy composites.*

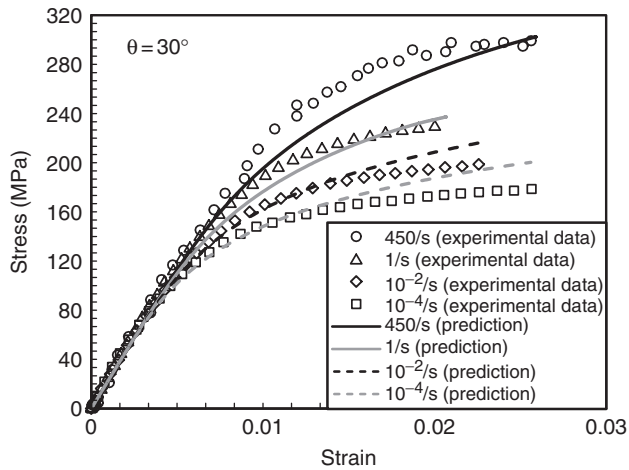

Figure 19. *Comparison of the experimental data with the model predictions for 30° graphite/epoxy composites.*

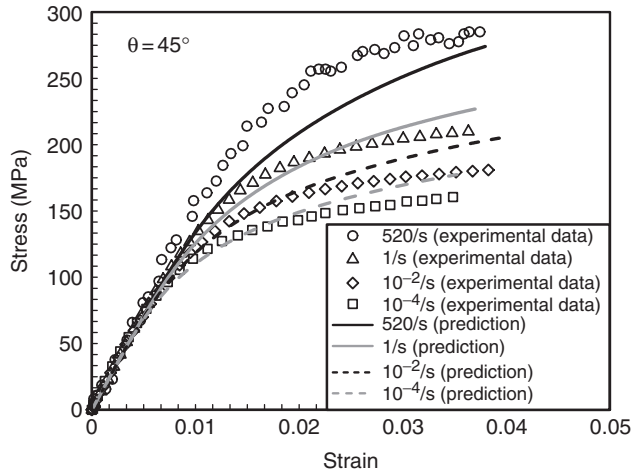

Figure 20. *Comparison of the experimental data with the model predictions for 45° graphite/epoxy composites.*

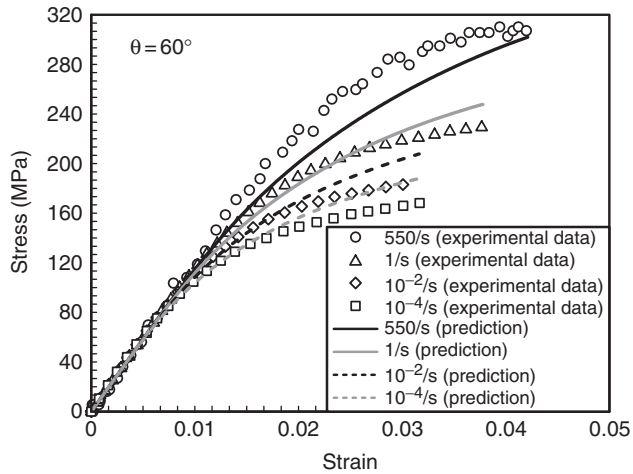

Figure 21. *Comparison of the experimental data with the model predictions for 60° graphite/epoxy composites.*

For comparison purposes, model predictions obtained from the GMC micromechanical analysis are also included in the figures. It is to be noted that the simulations were produced based on the material properties of HTA-12k graphite fiber together with the epoxy listed in Table 1. However, for the HTA-12k fiber, since only E_1 value was provided from the manufacturer, the other properties were evaluated such that the elastic constants obtained from the micromechanical model agree with their experimental counterparts.

Comparing the model predictions and experimental data suggests that the micromechanical model combined with the viscoplasticity behaviors of the epoxy are capable of describing the rate sensitivities of the off-axis specimens at a strain rate of up to 550/s.

Nevertheless, some discrepancies are observed between the experimental stress and strain curves and the model predictions. There are two possible reasons. The first is the assumption of a regular and periodic fiber array within the matrix. To alleviate the periodicity assumption of the composite microstructures, a more suitable representative volume element including random distributions of fiber needs to be proposed in the micromechanical analysis. However, in such a situation, more subcells and computation time are needed, a requirement that may not be practical to engineering applications. The second reason could be that the material properties of bulk epoxy may not be the same as the *in situ* matrix properties in the composites. It should be noted that, when the graphite fiber was incorporated with the epoxy resin, the morphology as well as the properties of the epoxy changed as a result of the interaction of the fibers and the polymer molecules. Although the implementation of the bulk epoxy properties may result in some deviations, this investigation can provide an indication of how rate-dependent behaviors of epoxy resin influence the mechanical responses of fiber composites, especially at high-strain-rate ranges.

CONCLUSIONS

The behaviors of graphite/epoxy composites, together with the rate-dependent behaviors of epoxy, were characterized using the GMC micromechanical model. The rate sensitivities of the epoxy resin were described using a three-parameter viscoplasticity model written in the form of power law. In the GMC analysis, it was found that the representative volume elements containing square fibers in a square array exhibit the same constitutive relations as that with round fibers. To validate the model predictions, off-axis graphite/epoxy composites were tested in compression at various strain rates using a conventional hydraulic MTS machine as well as the SHPB. Although some discrepancies existed between the model predictions and experimental data, it was concluded that the micromechanical approach developed is applicable to the establishment of a constitutive relation of graphite/epoxy composites at a strain rate up to 550/s.

ACKNOWLEDGMENTS

This research was supported by the National Science Council, Taiwan, under contract No. NSC 94-2212-E-009-017 to National Chiao Tung University.

REFERENCES

1. Sun, C.T. and Chen, J.L. (1989). A Simple Flow Rule for Characterizing Nonlinear Behavior of Fiber Composites, *Journal of Composite Materials*, **23**(10): 1009–1020.
2. Gates, T.S. and Sun, C.T. (1991). Elastic/Viscoplastic Constitutive Model for Fiber Reinforced Thermoplastic Composites, *AIAA Journal*, **29**(3): 457–463.
3. Yoon, K.J. and Sun, C.T. (1991). Characterization of Elastic-viscoplastic Properties of an AS4/PEEK Thermoplastic Composite, *Journal of Composite Materials*, **25**(10): 1277–1296.
4. Weeks, C.A. and Sun, C.T. (1998). Modeling Non-linear Rate-dependent Behavior in Fiber-reinforced Composites, *Composites Science and Technology*, **58**(3–4): 603–611.

5. Thiruppukuzhi, S.V. and Sun, C.T. (2001). Models for the Strain Rate Dependent Behavior of Polymer Composites, *Composites Science and Technology*, **61**(1): 1–12.
6. Eshelby, J.D. (1957). The Determination of the Elastic Field of an Ellipsoidal Inclusion, and Related Problems, In: *Proceedings of the Royal Society of London*, **A241**(1226): 376–396.
7. Mori, T. and Tanaka, K. (1973). Average Stress in Matrix and Average Elastic Energy of Materials with Misfitting Inclusions, *Acta Metallurgica*, **21**(5): 571–574.
8. Benveniste, Y. (1987). A New Approach to the Application of Mori–Tanaka Theory in Composite Materials, *Mechanics of Materials*, **6**(2): 147–157.
9. Sun, C.T. and Chen, J.L. (1991). A Micromechanical Model for Plastic Behavior of Fibrous Composites, *Composite Science and Technology*, **40**(2): 115–129.
10. Aboudi, J. (1982). A Continuum Theory for Fiber Reinforced Elastic Viscoplastic Composites, *International Journal of Engineering Science*, **20**(5): 605–621.
11. Aboudi, J. (1991). *Mechanics of Composite Materials – A Unified Micromechanical Approach*, Elsevier, New York.
12. Paley, M. and Aboudi, J. (1992). Micromechanical Analysis of Composites by the Generalized Cells Model, *Mechanics of Materials*, **14**(2): 127–139.
13. Pindera, M.J. and Bednarcyk, B.A. (1999). An Efficient Implementation of the Generalized Method of Cells for Unidirectional, Multi-phased Composites with Complex Microstructures, *Composites: Part B*, **30**(1): 87–105.
14. Ogihara, S., Kobayashi, S. and Reifsnider, K.L. (2003). Characterization of Nonlinear Behavior of Carbon/Epoxy Unidirectional and Angle-ply Laminates, *Advanced Composite Materials*, **11**(3): 239–254.
15. Goldberg, R.K. and Stouffer, D.C. (2002). Strain Rate Dependent Analysis of a Polymer Matrix Composite Utilizing a Micromechanics Approach, *Journal of Composite Materials*, **36**(7): 773–793.
16. Stouffer, D.C. and Dame, L.T. (1996). *Inelastic Deformation of Metals/Models, Mechanical Properties, and Metallurgy*, John Wiley & Sons, New York.
17. Robertson, D.D. and Mall, S. (1993) Micromechanical Relations for Fiber-reinforced Composites using the Free Transverse Shear Approach, *Journal of Composites Technology & Research*, **15**(3): 181–192.
18. Robertson, D.D. and Mall, S. (1994) Micromechanical Analysis for Thermoviscoplastic Behavior of Unidirectional Fibrous Composites, *Composites Science and Technology*, **50**(4): 483–496.
19. Kawai, M., Masuko, Y., Kawase, Y. and Negishi, R. (2001). Micromechanical Analysis of the Off Axis Rate-dependent Inelastic Behavior of Unidirectional AS4/PEEK at High Temperature, *International Journal of Mechanical Sciences*, **43**(9): 2069–2090.
20. Tsai, S.W. and Hahn, H.T. (1980). *Introduction to Composite Materials*, Technomic Publishing Company, Inc., Lancaster, Pennsylvania.
21. Lanza di Scalea, F. (1998). Measurement of Thermal Expansion Coefficients of Composites Using Strain Gages, *Experimental Mechanics*, **38**(4): 233–241.
22. Bing, Q. and Sun, C.T. (2004). A Technique for High Strain Rate SHPB Testing of Off-axis Carbon Fiber Composites, In: *The 11th European Conference on Composite Materials,* Rhodes, Greece.
23. Ninan, L., Tsai, J. and Sun, C.T. (2001). Use of Split Hopkinson Pressure Bar for Testing Off-axis Composites, *International Journal of Impact Engineering*, **25**(3): 291–313.
24. Graff, K.F. (1975). *Wave Motion in Elastic Solids*, Dover Publications, New York.